Optical and Quantum Electronics (2021) 53:237
https://doi.org/10.1007/s11082-021-02871-6

Low-pressure and liquid level fiber-optic sensor based on polymeric Fabry–Perot cavity

D. Jauregui-Vazquez[1] · M. E. Gutierrez-Rivera[2] · D. F. Garcia-Mina[3] · J. M. Sierra-Hernandez[1] · E. Gallegos-Arellano[4] · J. M. Estudillo-Ayala[1] · J. C. Hernandez-Garcia[1] · R. Rojas-Laguna[1]

Received: 6 September 2020 / Accepted: 11 April 2021 / Published online: 23 April 2021

Abstract
An experimental study of the interaction between a Mylar® polymer film and a multimode fiber-optic is presented for the simultaneous fiber-optic detection of low-pressure and liquid levels. The junction between the polymer and optical fiber produces an interference spectrum with maximal visibility and free spectral range around 9 dB and 31 nm, respectively. Water pressure, which is controlled by the liquid level, stresses the polymer. As a result, the spectrum wavelength shifts to the blue region, achieving high sensitivities around 2.49 nm/kPa and 24.5 nm/m. The polymeric membrane was analyzed using a finite element model; according to the results, the polymer shows linear stress response. Furthermore, the membrane material is operated below the yielding point. Moreover, the finite analysis provides information about the stress effect over the thickness and the birefringence changes. This sensor exhibits a quadratic polynomial fitting with an adjusted R-squared of 0.9539. The proposed sensing setup offers a cost-effective alternative for liquid level and low-pressure detection.

Keywords Fabry–Perot interferometer · Fiber optic sensor · Liquid level measurement · Pressure detection · Polymer

✉ D. Jauregui-Vazquez
jaureguid@ugto.mx

[1] Departamento de Ingeniería Electrónica, División de Ingenierías Campus Irapuato Salamanca, Universidad de Guanajuato, Carretera Salamanca- Valle de Santiago km 3.5 + 1.8 km, 36885 Salamanca, Gto., Mexico

[2] Departamento de Ingeniería Mecánica, División de Ingenierías Campus Irapuato Salamanca, Universidad de Guanajuato, Carretera Salamanca- Valle de Santiago km 3.5 + 1.8 km, 36885 Salamanca, Gto., Mexico

[3] Departamento de Física, Facultad de Ciencias Básicas, Universidad Autónoma de Occidente, Calle 25 # 115-85, Cali 760030, Colombia

[4] Departamento de Mecatrónica, Universidad Tecnológica de Salamanca, Av. Universidad Tecnológica #200, Col. Ciudad Bajío, C.P. 36766 Salamanca, Gto., Mexico

1 Introduction

Low-pressure and liquid levels are essential parameters for the oil-gas, food, and chemical industries. Also, low-pressure is a crucial factor to be estimated in several medical procedures (Leitão et al. 2016; Marques et al. 2017; Sartiano and Sales 2017; Shin et al. 2019; Wolthuis et al. 1991). Therefore, many optical devices have been proposed to satisfy this demand (Escudero et al. 2019; Kim et al. 2018; Lacam and Chateau 1989; Leger et al. 1990; Musayev and Karlik 2003). Among these proposals, fiber-optic sensors have been demonstrated as a reliable alternative to conduct the independent or simultaneous detection of liquid levels and pressure.

One of the most common methods used to detect pressure is optical fiber Fabry–Perot Interferometer structure (FPI) (Abeysinghe et al. 2001; Bai et al. 2016; Spillman 1982; Vorathin et al. 2020; Wang et al. 2006a, b). These structures can be classified according to the cavity formation, such as intrinsic and extrinsic FPI sensors. The most common extrinsic Fabry–Perot fiber optic structure used for pressure sensing applications employs Micro Electro Mechanical Systems (MEMS) (Abeysinghe et al. 2001; Li et al. 2006; Qi et al. 2019; Wang et al. 2006a, b). The adequate performance of these structures has been widely demonstrated. However, its manufacturing process involves intricate micromachining and chemical processes. Meanwhile, some intrinsic Fabry–Perot fiber-optic structures have been proposed and demonstrated for pressure detection using the arc splice technique. Most of these techniques combine a solid core fiber and air-silica fiber optic structure to produce an intrinsic air cavity (Ma et al. 2011; Yu et al. 2015; Zhang et al. 2019). These devices are compact and versatile; however, the number of steps required to achieve the structure reduces its repeatability under the same splicing parameters. Other low-cost methods have been demonstrated using etched fiber optics and polymer adhesive (Chen et al. 2017), or by merely adding special adhesive at the tip of conventional fibers (Oliveira et al. 2019; Zhang et al. 2017), as well as combining long polymer membranes with high reflective material at the fiber's tip (Zhu et al. 2017).

Currently, most of the proposed fiber optic sensors to estimate liquid level are based on inline, all-fiber structures, such as tapered fibers (Hsu et al. 2013), Mach–Zehnder Interferometers (Liu et al. 2020; Sun et al. 2015), Michelson Interferometers (Li et al. 2018) , and Multimode interferometers (Antonio-Lopez et al. 2011). These structures can be easily adapted to the sensing region. However, some of them present highly phase modulation responses for more than one parameter. As a result, crosstalk measurement and instabilities could occur.

It is worth stressing that some works have combined the benefits of extrinsic Fabry–Perot interferometers to detect liquid levels (Diaz et al. 2019; Lü and Yang 2007; Wang and Li 2014). It is necessary to notice that the membrane material is a key aspect of designing an FPI sensor for pressure detection. This parameter will govern the sensitivity, dynamic range, and temperature operation. A hard-solid membrane may reduce the possibility of monitoring the low-pressure range, considering that the low-pressure range is < 10 kPa (Srivastava and Chattopadhyay 2017).

In this work, an alternative method to detect pressure and liquid level is presented. The technique is based on an extrinsic Fabry–Perot structure produced by the junction between a multimode fiber optic and a Mylar® polymer film. The soft properties of the material allow the detection of low-pressure levels with high sensitivity and good resolution. The present technique is a cost-effective alternative to detect pressure and liquid levels, considering the wavelength operation and the materials involved.

2 Theory

The proposed low-pressure and liquid level multimode fiber-optic sensor is based on the refractive index interface generated by the junction between a thin Mylar® polymer film (MPF) and a multimode fiber-optic (MMF). The schematic interaction between the polymer and the multimode fiber optic is presented in Fig. 1.

When the light in the MMF arrives at the MPF, one part is transmitted, and the rest is reflected. The refractive index interface causes the first reflection between n_1 (1.468 − MMF) and n_2 (1.67 − MPF). It is worth noting that the reflection can be estimated by the Fresnel relation, $R_1 = (n_1 - n_2/\, n_2 + n_1)^2$. The transmitted light portion goes through the MPF cavity and reaches the second refractive index interface, generated between n_2 and n_3 (surrounding environment). Here, the following reflection occurs: $R_2 = (n_2 - n_3/n_3 + n_2)^2$. The one-layer Fabry–Perot expression governs the interaction of these reflections (Van De Stadt and Muller 1985; Zhao et al. 2018):

$$I_R(\lambda) = R_1 + (1-\alpha)^2(1-\beta)^2(1-R_1)^2R_2 + 2(1-\alpha)(1-\beta)\left(R_1R_2\right)^{\frac{1}{2}}\cos(4\pi\Delta nd/\lambda) \tag{1}$$

where α and β represent the transmitted and the cavity losses, respectively, the round-trip phase is described in terms of d-cavity distance (thickness of the MPF), n_c cavity's refractive index, and λ wavelength operation.

However, when pressure is applied at one lateral face of the MPF, the membrane is deflected. As a result, the material is stressed. In our case, when water pressure was applied in the opposite direction of the MMF, the Fabry–Perot cavity was altered; then, the pumped light into the MMF reached over the stressed material (see Fig. 2a).

The deflection generated by the water pressure can be analyzed using a cylindrical coordinate system (see Fig. 2b). Hence, the stress in the radial (σ_r) and angular (σ_θ) components can be described by the following relations (Reddy 2006):

$$\sigma_r(r,z) = \frac{3qa^2z}{4d^3}\left[(1+\nu) - (3+\nu)r^2/a^2\right] \tag{2a}$$

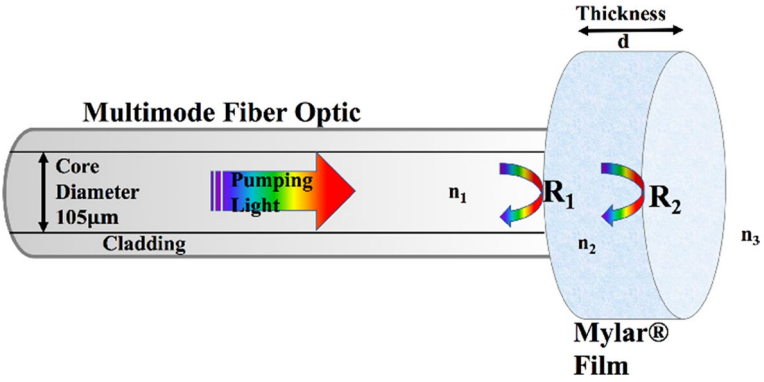

Fig. 1 Illustration of the junction between the Mylar® polymer film and the multimode fiber optic

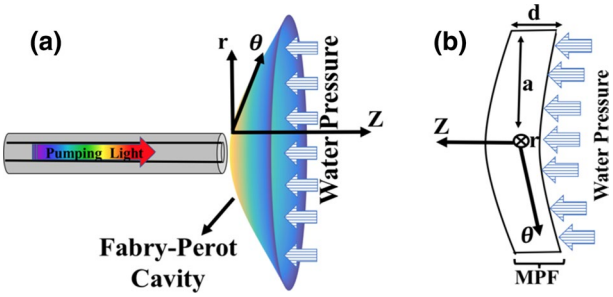

Fig. 2 **a** Deflection membrane by water pressure applied and **b** cylindrical system coordinates for the MPF and MMF interaction

$$\sigma_r(r,z) = \frac{3qa^2z}{4d^3}\left[(1+\nu) - (1+3\nu)r^2/a^2\right] \tag{2b}$$

here, d is the cavity thickness, a is the membrane's radii, and q is the transversal load applied by the water pressure. The material properties are represented by Poisson's ratio (ν). It can be seen that both stresses will depend on the polymer displacement (Z), the water pressure applied (expressed by the load q), as well the coordinates (r, Z). Furthermore, both stresses decreased as the radii (a) increased. As a result, a stress difference occurred in the radial directions (r, θ, Z), presenting an anisotropy optical medium. Then, the induced birefringence can be estimated by (Urbańczyk and Pietraszkiewicz 1988):

$$\Delta n = C\Delta\sigma \tag{3}$$

In the last relation, C is the polymer's elastic-optic coefficient, and $\Delta\sigma$ is the stress difference between the analyzed components; for this case, $\Delta\sigma$ is the difference between σ_r and σ_z. This refractive index variation modifies the round trip presented in Eq. 1. It is worth noting that the water pressure and liquid level are related by $P = \rho gh$, in which the well-known acceleration of gravity (g) and water density (ρ) constants are involved; thus, it is possible the estimation about the liquid level that originates the pressure.

3 Experimental setup

The experimental setup shown in Fig. 3 was employed to demonstrate the water pressure and liquid level detection. An interrogation multimode fiber optic setup was implemented. The spectrometer and an incandescent lamp were interconnected using a 50/50 multimode fiber coupler (TM105R5F1A).

A container was also manufactured to fix a commercial 3.6 μm thickness polymer film used to detect the pressure and liquid level (see Fig. 4). The container was a cube with a 5-inch edge length. A hole was drilled in one face of the container, where the Mylar® film was fixed using special glue; the total membrane diameter is 12.7 mm. At the same position, on the opposite face, a manometer was set to monitor the pressure. At this point, a valve was located to control the liquid level. A pipe with a scale was placed at the top of the box/container. At this point, the liquid level was monitored as the water was added. As the liquid level increased, the pressure at the bottom of the container increased; Here, the manometer monitored the pressure at the same position as the polymer. The water increment caused the soft polymer to deflect and to be stressed. An optical fiber FC/PC connector was used to incite the MMF and MPF interaction. This connector was set over a translation stage and fixed using a fiber holder.

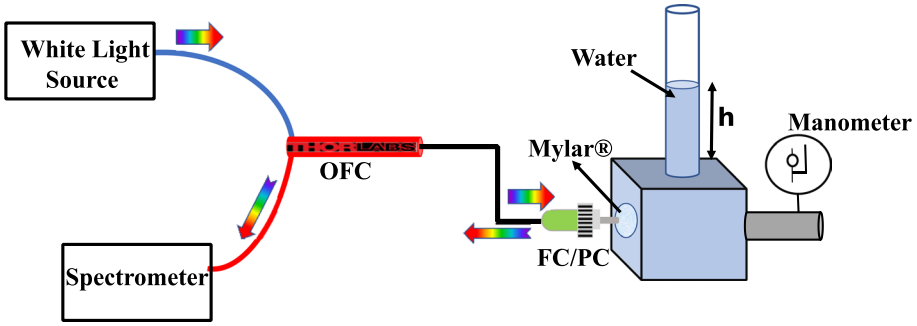

Fig. 3 **a** Polymer spectrum response after and before water interaction. **b** Computed reflection response of polymer Fabry–Perot cavity

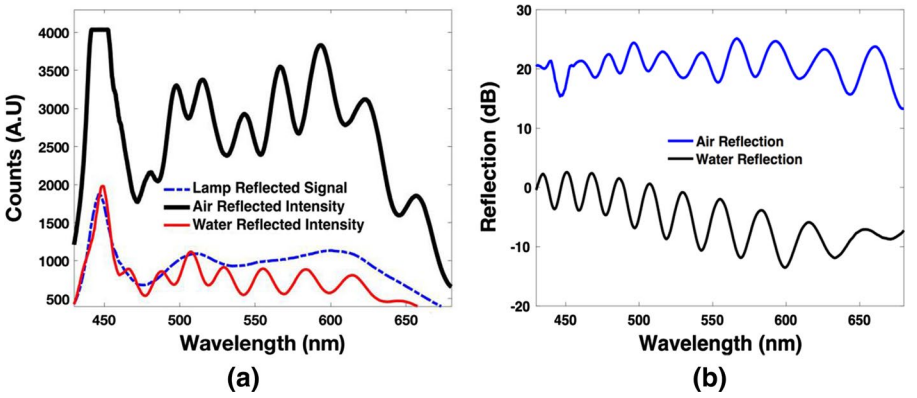

Fig. 4 Experimental setup

The junction between the MPF and MMF produced the interference spectrum shown in Fig. 3a. This spectrum is achieved before the water is added into the container. The power intensity increment was generated by the Mylar's high refractive index (1.67). However, the reflection R_2 decreased around five times, when the surrounding refractive index went from $n_3 = 1.0$(air) to $n_3 = 1.3329$ (water), resulting in a decline of all the interference signals. Despite this decreased power level, the interference spectrum was significantly observed. Moreover, it is worth mentioning that no significant liquid level was evident when the membrane was completely covered by water. Furthermore, by considering the interference spectrum when the MPF is surrounded by air, it can be assumed that α and β from Eq. 1 can be ignored. The total power reflection generated by the MPF and MMF interaction is computed and presented in Fig. 3b. The presented spectrums correspond to the surrounding medium of water and air. These interference spectrums present minimal and maximal visibility (V) of 3 and 9 dB, respectively. The Free Spectral Range (FSR) of both spectrums vary from 21 to 31 nm. This linear increment response is related to the following expression:

$$FSR = \left(\lambda_1 - \lambda_2\right) = \frac{\left(\lambda_1 \lambda_2\right)^2}{2 n_c d} \tag{4}$$

where λ_1 and λ_2 represent the adjacent deep wavelength points of an interference peak. Considering the following parameters of the air reflection spectrum: $\lambda_{1a} = 578.7$, $\lambda_{2a} = 608.9$, cavity's refractive index $n_2 = 1.67$, and cavity thickness of $d = 3.6$ µm, the FSR can be estimated around 29.3 nm. However, considering the difference between the adjacent points, the FSR is around 30.2 nm; this FSR corresponds to a Fabry–Perot cavity length close to 3.493 µm. The difference between the manufacture data thickness and the thickness computed in this work can be attributed to the stress applied at the moment of fixing the polymer; moreover, the interaction between the MPF and multimode fiber connector also induces minimal stress. Both aspects produce a difference between the analyzed FSR. However, when the polymer is completely covered by water, the FSR is altered; and moreover, a wavelength shifting is presented.

The following points of the water reflection spectrum are shown in Fig. 3b: $\lambda_{1w} = 569.1$ and $\lambda_{2w} = 600.1$; an FSR around 31 nm is computed. By a constant cavity's refractive index (1.67), the cavity's length can be estimated at around 3.298 µm; However, this implies a considerable reduction of the initial Fabry–Perot cavity length (3.493 µm). Nevertheless, considering the cavity length as a constant (3.493 µm), a cavity's refractive index of 1.5767 is computed. This alteration is more suitable for the experiment, and the refractive index change can be related to mechanical properties alteration when the polymer when is covered by water (Volynskii and Bakeev 2018).

Moreover, according to the Mylar® properties, the absorption value is close to 0.8 % after immersing the polymer in water for 24 h (http://usa.dupontteijinfilms.com/wp content/uploads/2017/01/Mylar_Chemical_Properties.pdf). It is essential to notice that this absorption is the maximal saturation value. By using the cavity length, the refractive index of the cavity, and the Fresnel reflections analyzed above; it is possible to analyze and compare the Fabry–Perot response for water and air surrounding medium; these data are used in Eq. 1 for both cases (see Fig. 5).

As can be appreciated in Fig. 5, the power level and the FSR are very similar to the data presented in Fig. 3b. The visibility variation is related to the wavelength refractive index dependence and the stress presented in both cases. Furthermore, a Finite Element Model (FEM) was carryout by using ANSYS software. Here, the membrane dimensions and the following parameters are used: $E = 4.8956$ MPa and $\nu = 0.38$; as a result, it is possible to

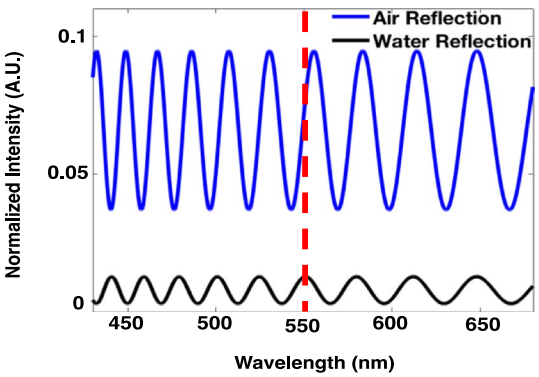

Fig. 5 Computed reflection response of Fabry–Perot cavity surrounded by air and water

know the stress in the cylindrical coordinates; the stress values as well the thickness membrane variation are presented in Table 1.

The ANSYS model reveals a significant stress difference between σ_r and σ_z; moreover, the radial and theta directions' stress are the same. It is important to notice that the refractive index alterations caused by the stress changes are limited by the elastic-optic coefficient (C), which is not available for the polymer sample. However, considering Eq. 3, a refractive index alteration can be expected when the membrane is stressed by external low-pressure. Moreover, it can be assumed that the sensor's operations are mostly governed by the birefringence effect generated by the stress difference in the radial and displacement coordinates. Hence, it is crucial to notice that the maximal thickness variation (17 nm) represents a minimal variation and contribution to the phase variation.

4 Results

Once the system operation is validated, the water liquid level is increased in the container; consequently, the pressure also increases, the mentioned relation, $P = \rho gh$ link both. Indeed, considering the manometer's pressure, the liquid level can be compared to the scale set at the pipe container.

As the water is added to the container through the pipe, the interference spectrum exhibited a clear wavelength shift to the blue region (see Fig. 6). Then, the interference spectrum shifted, the visibility varied in a nonlinear manner. Thus, this parameter was not analyzed for sensing purposes. When the maximal pressure (6.20 kPa) was applied, a total signal shifting of around $\pi/2$ was observed, and some interference points changed the color region. In order to analyze the sensitivity and color change, the peaks (P1 = 555 nm and P2 = 528.7 nm) and depths (D1 = 568.78 nm and D2 = 541.22 nm) presented in Fig. 6 were analyzed and compared in Fig. 7a.

These points exhibited very similar responses. Moreover, a maximal wavelength shifting of around 13.2 nm (P1) was achieved; Thus, the following maximal sensitivities can be expected by P1: 2.72 nm/kPa, and 26.77 nm/m. Despite its adequate power level and visibility, this point's shifting did not present a color region change, desired to reduce its cost for future implementation. On the other hand, D1 presented a sensitivity of 2.49 nm/kPa and 24.5 nm/m. Therefore, given the spectrometer's resolution (1 nm), a competitive resolution of around 0.40 kPa and 0.04 m was achieved. Even with the sensitivity and the

Table 1 Stress and thickness ANSYS model response for low-pressure variation

p (kPa)	σr (Pa)	σz (Pa)	Δ thickness
0.50	7,875,080	0.2787	3E−09
1.00	12,484,900	0.4485	5E−09
1.50	16,354,900	0.5926	8E−09
2.00	19,812,600	0.7225	9E−09
2.50	22,993,800	0.8429	1.1E−08
3.00	25,971,200	0.9563	1.2E−08
3.50	28,789,500	1.0643	1.3E−08
4.00	31,478,800	1.1679	1.5E−08
4.50	34,060,400	1.2679	1.5E−08
5.00	36,550,100	1.3648	1.7E−08

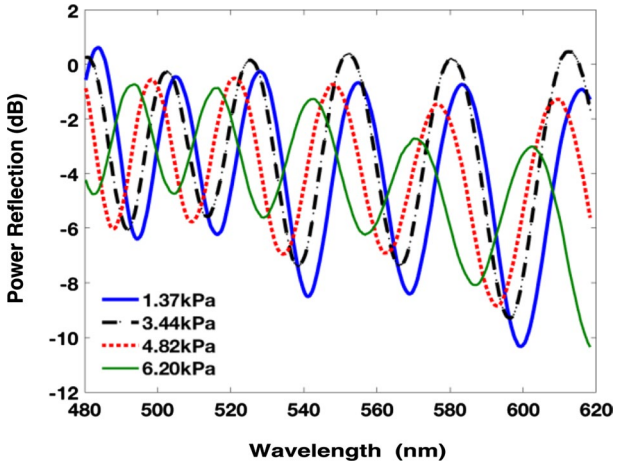

Fig. 6 Interference spectrum response for water pressure variation

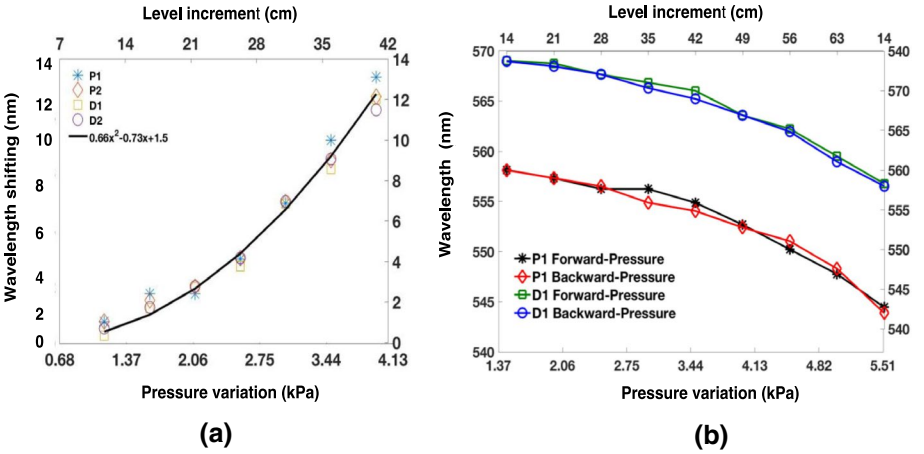

Fig. 7 **a** Wavelength shifting of the peaks and depths: P1 = 555 nm, P2 = 528.7 nm, D1 = 568.78 nm, and D2 = 541.22 nm. **b** Hysteresis analysis of the analyzed points

power level presented, this point (D1) presented a significant color change from yellow to green. Moreover, this peak exhibited a quadratic polynomial fitting with an adjusted R-squared of 0.9539.

To evaluate the hysteresis, we slowly removed the water from the container. Then, the interference points P1 and D1 were analyzed and compared in Fig. 7b. As can be appreciated, depth D1 presented minimal error; here, the trajectory had a path difference of 1 nm. Furthermore, the interference was monitored to validate the sensing setup; here, constant pressure of 1.37 kPa was applied. The power and wavelength fluctuations presented by D1 are presented in Fig. 8. As can be observed, the maximal wavelength fluctuation is around 1 nm, then the maximal error measurement during the time can be estimated around 0.17%. The power fluctuations can be ignored because of the minimal variation, and modulation analyzed in this work.

It is important to stress that the analyte refractive index variation is limited by the container design. However, if a refractive index change is presented, it can be expected

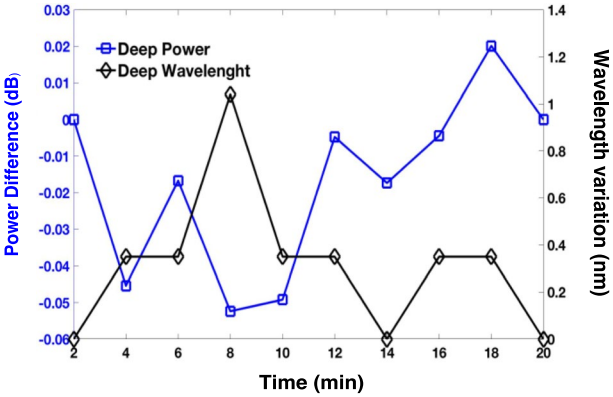

Fig. 8 Stability analysis

a visibility variation; this is assumed by considering the Fresnel reflection equation. It is important to point out that the results described above were achieved in a room temperature of 22 °C. Even though the MPF has a melting point close to 254 °C (Sanaâ et al. 2016), there could be some thermal effects that could affect the adhesive used to fix the polymer, as well possible degradation of the polymer chains. Therefore, it is suggested that the sensing temperature operation should be carried out at room temperature. Despite these challenges, the proposed system offers a competitive sensitivity and resolution. The results are compared with prior works in Table 2 (pressure) and Table 3 (liquid level).

Table 2 Comparative pressure sensitivity results considering prior works

Reference	Range (kPa)	Sensitivity (nm/kPa)
Tian et al. (2012)	0–41	1.451
Guo et al. (2019)	96–1654	0.419
Lin and Fang (2016)	0-255	1.30
Zhang et al. (2017)	0–60	0.065
Ma et al. (2017)	0–50	0.198
Zhang et al. (2020)	0–200	0.062
This work	0–6.89	2.49

Table 3 Liquid level sensitivity comparison with prior works

References	Range (m)	Sensitivity (nm/m)
Vorathin et al. (2019)	0–2	2.53
Martins et al. (2019)	0–0.9	4.4
Diáz et al. (2018)	0–0.5	2.74
Ameen et al. (2016)	0–1	2.48
Castellani et al. (2017)	0–0.12	6
This work	0.14–0.70	24.5

5 Conclusions

The interaction between a multimode fiber-optic and a Mylar® polymer film, using a pumped visible light spectrum, is demonstrated as a low-cost fiber optic sensor for pressure and liquid level monitoring. This union functions as a one-layer Fabry–Perot cavity. Here, its response is governed by the stresses applied over the polymer film. The water liquid level controls these stresses in the sensing setup, in which a scale and a manometer, respectively, were used to monitor the liquid level and water pressure. Moreover, both of them are compared by the pressure and density relationship for fluids. When the liquid level and water pressure are altered, the spectrum undergoes a wavelength shift to a shorter wavelength. The best wavelength operation was presented by a depth centered at 568.78 nm, where sensitivities of 2.49 nm/Pa and 24.5 nm/m were achieved. As a result, high resolutions of around 0.40 kPa and 0.04 m are obtained for pressure and level, respectively. The sensing setup presents a quadratic polynomial fitting with an adjusted R-squared of 0.9539. Furthermore, The hysteresis and stability analyses reveal minimal error measurements (1 nm and 0.17%, respectively). This sensor offers a cost-effective implementation, as well as high resolution and sensitivity. Monitoring low-pressure is strongly related to medical procedures; the results achieved can be an alternative for drug infusion monitoring, hyperbaric therapy, and medical ventilators.

Acknowledgements This work was partially supported by IDEA GTO throughout the project AI-20-37. D. Jauregui-Vazquez is thankful with his family for their support during the quarantine COVID-19.

Disclosures The authors declare no conflicts of interest. Moreover, the idea presented is original and it is not under consideration for publication in other editorial/journal.

References

Abeysinghe, D.C., Dasgupta, S., Boyd, J.T., Jackson, H.E.: A novel MEMS pressure sensor fabricated on an optical fiber. IEEE Photonics Technol. Lett. **13**, 993–995 (2001). https://doi.org/10.1109/68.942671

Ameen, O.F., Younus, M.H., Aziz, M.S., Azmi, A.I., Raja Ibrahim, R.K., Ghoshal, S.K.: Graphene diaphragm integrated FBG sensors for simultaneous measurement of water level and temperature. Sensors Actuators A Phys. **252**, 225–232 (2016). https://doi.org/10.1016/j.sna.2016.10.018

Antonio-Lopez, J.E., Sanchez-Mondragon, J.J., LiKamWa, P., May-Arrioja, D.A.: Fiber-optic sensor for liquid level measurement. Opt. Lett. **36**, 3425–3427 (2011). https://doi.org/10.1364/OL.36.003425

Bai, Y., Yan, F., Liu, S., Wen, X.: All fiber Fabry–Pérot interferometer for high-sensitive micro-displacement sensing. Opt. Quantum Electron. **48**, 1–10 (2016). https://doi.org/10.1007/s11082-015-0323-y

Castellani, C.E.S., Ximenes, H.C.B., Silva, R.L., Frizera-Neto, A., Ribeiro, M.R.N., Pontes, M.J.: Multiparameter interferometric sensor based on a reduced diameter core axial offseted fiber. IEEE Photonics Technol. Lett. **29**, 239–242 (2017). https://doi.org/10.1109/LPT.2016.2637870

Chen, W.P., Wang, D.N., Xu, B., Zhao, C.L., Chen, H.F.: Multimode fiber tip Fabry–Perot cavity for highly sensitive pressure measurement. Sci. Rep. **7**, 1–6 (2017). https://doi.org/10.1038/s41598-017-00300-x

Diáz, C.A.R., Leal-Junior, A.G., André, P.S.B., Da Costa Antunes, P.F., Pontes, M.J., Frizera-Neto, A., Ribeiro, M.R.N.: Liquid level measurement based on FBG-embedded diaphragms with temperature compensation. IEEE Sens. J. **18**, 193–200 (2018). https://doi.org/10.1109/JSEN.2017.2768510

Diaz, C.A.R., Leal-Junior, A., Marques, C., Frizera, A., Pontes, M.J., Antunes, P.F.C., Andre, P.S.B., Ribeiro, M.R.N.: Optical fiber sensing for sub-millimeter liquid-level monitoring: a review. IEEE Sens. J. **19**, 7179–7191 (2019). https://doi.org/10.1109/JSEN.2019.2915031

Escudero, P., Yeste, J., Pascual-Izarra, C., Villa, R., Alvarez, M.: Color tunable pressure sensors based on polymer nanostructured membranes for optofluidic applications. Sci. Rep. **9**, 1–10 (2019). https://doi.org/10.1038/s41598-019-40267-5

Guo, Z., Lv, W., Wang, W., Chen, Q., Zhang, X., Chen, H., Ma, Z.: Absolute single cavity length interrogation of fiber-optic compound Fabry–Perot pressure sensors through a white light non-scanning correlation method. Sensors (Switzerland). (2019). https://doi.org/10.3390/s19071628

Hsu, J., Lee, C., Chang, H., Shih, W.C., Li, C.: Highly sensitive tapered fiber Mach–Zehnder interferometer for liquid level sensing. IEEE Photonics Technol. Lett. **25**, 1354–1357 (2013). https://doi.org/10.1109/LPT.2013.2265738

Kim, J.T., Choi, H., Shin, E.J., Park, S., Kim, I.G.: Graphene-based optical waveguide tactile sensor for dynamic response. Sci. Rep. **8**, 1–6 (2018). https://doi.org/10.1038/s41598-018-34613-2

Lacam, A., Chateau, C.: High-pressure measurements at moderate temperatures in a diamond anvil cell with a new optical sensor: SrB4O7:Sm2+. J. Appl. Phys. **66**, 366–372 (1989). https://doi.org/10.1063/1.343884

Leger, J.M., Chateau, C., Lacam, A.: SrB4O7:Sm2 + pressure optical sensor: Investigations in the megabar range. J. Appl. Phys. **68**, 2351–2354 (1990). https://doi.org/10.1063/1.346543

Leitão, C., Antunes, P., Pinto, J., Mesquita Bastos, J., André, P.: Optical fiber sensors for central arterial pressure monitoring. Opt. Quantum Electron. **48**, 1–9 (2016). https://doi.org/10.1007/s11082-016-0494-1

Li, M., Wang, M., Li, H.: Optical MEMS pressure sensor based on Fabry–Perot interferometry. Opt. Express. **14**, 1497 (2006). https://doi.org/10.1364/oe.14.001497

Li, P., Yan, H., Zhang, H.: Highly sensitive liquid level sensor based on an optical fiber Michelson interferometer with core-offset structure. Optik (Stuttg). **171**, 781–785 (2018). https://doi.org/10.1016/j.ijleo.2018.06.126

Lin, C., Fang, X.: Miniature MEMS Fabry–Perot interferometry pressure sensor and the fabrication system. In: 2016 10th IEEE International Conference on Anti-counterfeiting, Security, and Identification (ASID), pp. 105–108 (2016). https://doi.org/10.1109/ICASID.2016.7873927

Liu, Q., He, X., Fu, H., Yang, D., Xiao, F., Wang, X.: Temperature-insensitive optical fiber reflective micro-liquid level sensor base on the drop shape quasi-Mach Zehnder interferometer. Optik (Stuttg). **216**, 164893 (2020). https://doi.org/10.1016/j.ijleo.2020.164893

Lü, T., Yang, S.: Extrinsic Fabry–Perot cavity optical fiber liquid-level sensor. Appl. Opt. **46**, 3682–3687 (2007). https://doi.org/10.1364/AO.46.003682

Ma, J., Ju, J., Jin, L., Jin, W.: A compact fiber-tip micro-cavity sensor for high-pressure measurement. IEEE Photonics Technol. Lett. **23**, 1561–1563 (2011). https://doi.org/10.1109/LPT.2011.2164060

Ma, Z.M., Huang, Y.W., Meng, H., Huang, X.G.: Simultaneous measurement of temperature and pressure by utilizing an integrated Mach–Zehnder. J. Light. Technol. **35**, 4924–4929 (2017). https://doi.org/10.1109/JLT.2017.2765278

Marques, C.A.F., Webb, D.J., Andre, P.: Polymer optical fiber sensors in human life safety. Opt. Fiber Technol. **36**, 144–154 (2017). https://doi.org/10.1016/j.yofte.2017.03.010

Martins, J., Diaz, C.A.R., Domingues, M.F., Ferreira, R.A.S., Antunes, P., Andre, P.S.: Low-cost and high-performance optical fiber-based sensor for liquid level monitoring. IEEE Sens. J. **19**, 4882–4888 (2019). https://doi.org/10.1109/JSEN.2019.2895549

Musayev, E., Karlik, S.E.: A novel liquid level detection method and its implementation. Sensors Actuators A Phys. **109**, 21–24 (2003). https://doi.org/10.1016/S0924-4247(03)00347-9

Oliveira, R., Bilro, L., Nogueira, R., Rocha, A.M.: Adhesive based Fabry-Pérot hydrostatic pressure sensor with improved and controlled sensitivity. J. Light. Technol. **37**, 1909–1915 (2019). https://doi.org/10.1109/JLT.2019.2894949

Qi, X., Wang, S., Jiang, J., Liu, K., Wang, X., Yang, Y., Liu, T.: Fiber optic Fabry–Perot pressure sensor with embedded MEMS micro-cavity for ultra-high pressure detection. J. Light. Technol. **37**, 2719–2725 (2019). https://doi.org/10.1109/JLT.2018.2876717

Reddy, J.N.: Theory and Analysis of Elastic Plates and Shells, Second Edition. Taylor & Francis (2006). https://doi.org/10.1201/9780849384165

Sanaâ, F., Palierne, J.F., Gharbia, M.: Channelled spectrum method for birefringence dispersion measurement of anisotropic Mylar film. Opt. Mater. (Amst). **57**, 193–201 (2016). https://doi.org/10.1016/j.optmat.2016.04.036

Sartiano, D., Sales, S.: Low cost plastic optical fiber pressure sensor embedded in mattress for vital signal monitoring. Sensors (Switzerland). (2017). https://doi.org/10.3390/s17122900

Shin, J., Liu, Z., Bai, W., Liu, Y., Yan, Y., Xue, Y., Kandela, I., Pezhouh, M., MacEwan, M.R., Huang, Y., Ray, W.Z., Zhou, W., Rogers, J.A.: Bioresorbable optical sensor systems for monitoring of intracranial pressure and temperature. Sci. Adv. **5**, 1–13 (2019). https://doi.org/10.1126/sciadv.aaw1899

Spillman, W.B.: Multimode fiber-optic pressure sensor based on the photoelastic effect. Opt. Lett. **7**, 388 (1982). https://doi.org/10.1364/ol.7.000388

Srivastava, R., Chattopadhyay, J.: Design and Fabrication of Nanomaterial-Based Device for Pressure Sensorial Applications BT - Advanced Nanomaterials in Biomedical, Sensor and Energy Applications. (2017). https://doi.org/10.1007/978-981-10-5346-7

Sun, M., Jin, Y., Dong, X.: All-Fiber Mach–Zehnder Interferometer for Liquid Level Measurement. IEEE Sens. J. **15**, 3984–3988 (2015). https://doi.org/10.1109/JSEN.2015.2406872

Tian, J., Zhang, Q., Fink, T., Li, H., Peng, W., Han, M.: Tuning operating point of extrinsic Fabry–Perot interferometric fiber-optic sensors using microstructured fiber and gas pressure. Opt. Lett. **37**, 4672–4674 (2012). https://doi.org/10.1364/OL.37.004672

Urbańczyk, W., Pietraszkiewicz, K.: Measurements of stress anisotropy in fiber preform: modification of the dynamic spatial filtering technique. Appl. Opt. **27**, 4117 (1988). https://doi.org/10.1364/ao.27.004117

Van De Stadt, H., Muller, J.M.: Multimirror Fabry–Perot interferometers. J. Opt. Soc. Am. A. **2**, 1363–1370 (1985). https://doi.org/10.1364/JOSAA.2.001363

Volynskii, L., Bakeev, N.F.: Surface Phenomena in the Structural and Mechanical Behaviour of Solid Polymers. CRC Press (2018). https://doi.org/10.1201/9781315367873

Vorathin, E., Hafizi, Z.M., Aizzuddin, A.M., Zaini, M.K.A., Lim, K.S.: A novel temperature-insensitive hydrostatic liquid-level sensor using chirped FBG. IEEE Sens. J. **19**, 157–162 (2019). https://doi.org/10.1109/JSEN.2018.2875532

Vorathin, E., Hafizi, Z.M., Ismail, N., Loman, M.: Review of high sensitivity fibre-optic pressure sensors for low pressure sensing. Opt. Laser Technol. (2020). https://doi.org/10.1016/j.optlastec.2019.105841

Wang, W., Li, F.: Large-range liquid level sensor based on an optical fibre extrinsic Fabry–Perot interferometer. Opt. Lasers Eng. **52**, 201–205 (2014). https://doi.org/10.1016/j.optlaseng.2013.06.009

Wang, X., Li, B., Russo, O.L., Roman, H.T., Chin, K.K., Farmer, K.R.: Diaphragm design guidelines and an optical pressure sensor based on MEMS technique. Microelectronics J. 37, 50–56 (2006a). https://doi.org/10.1016/j.mejo.2005.06.015

Wang, X., Xu, J., Zhu, Y., Cooper, K.L., Wang, A.: All-fused-silica miniature optical fiber tip pressure sensor. Opt. Lett. 31, 885–887 (2006b). https://doi.org/10.1364/OL.31.000885

Wolthuis, R.A., Mitchell, G.L., Saaski, E., Hartl, J.C., Afromowitz, M.A.: Development of medical pressure and temperature sensors employing optical spectrum modulation. IEEE Trans. Biomed. Eng. **38**, 974–981 (1991). https://doi.org/10.1109/10.88443

Yu, Y., Chen, X., Huang, Q., Du, C., Ruan, S., Wei, H.: Enhancing the pressure sensitivity of a Fabry–Perot interferometer using a simplified hollow-core photonic crystal fiber with a microchannel. Appl. Phys. B. **120**, 461–467 (2015). https://doi.org/10.1007/s00340-015-6155-4

Zhang, L., Jiang, Y., Gao, H., Jia, J., Cui, Y., Ma, W., Wang, S., Hu, J.: A diaphragm-free fiber Fabry–Perot gas pressure sensor. Rev. Sci. Instrum. **90**, 25005 (2019). https://doi.org/10.1063/1.5055660

Zhang, Q., Lei, J., Chen, Y., Wu, Y., Xiao, H.: Glass 3D printing of microfluidic pressure sensor interrogated by fiber-optic refractometry. IEEE Photonics Technol. Lett. **32**, 414–417 (2020). https://doi.org/10.1109/LPT.2020.2977324

Zhang, Z., Liao, C., Tang, J., Bai, Z., Guo, K., Hou, M., He, J., Wang, Y., Wang, Y., Liu, S., Zhang, F.: High-sensitivity gas-pressure sensor based on fiber-tip PVC diaphragm Fabry-Pérot interferometer. J. Light. Technol. **35**, 4067–4071 (2017). https://doi.org/10.1109/JLT.2017.2710210

Zhao, Y., Yuan, Y., Gan, W., Yang, M.: Optical fiber Fabry–Perot humidity sensor based on polyimide membrane: sensitivity and adsorption kinetics. Sensors Actuators A Phys. **281**, 48–54 (2018). https://doi.org/10.1016/j.sna.2018.08.044

Zhu, J., Wang, M., Chen, L., Ni, X., Ni, H.: An optical fiber Fabry–Perot pressure sensor using corrugated diaphragm and angle polished fiber. Opt. Fiber Technol. **34**, 42–46 (2017). https://doi.org/10.1016/j.yofte.2016.12.004